Impact of Social Distancing Measures on Coronavirus Disease Healthcare Demand, Central Texas, USA

Xutong Wang,[1] Remy F. Pasco,[1] Zhanwei Du,[1] Michaela Petty, Spencer J. Fox, Alison P. Galvani, Michael Pignone, S. Claiborne Johnston, Lauren Ancel Meyers

Social distancing orders have been enacted worldwide to slow the coronavirus disease (COVID-19) pandemic, reduce strain on healthcare systems, and prevent deaths. To estimate the impact of the timing and intensity of such measures, we built a mathematical model of COVID-19 transmission that incorporates age-stratified risks and contact patterns and projects numbers of hospitalizations, patients in intensive care units, ventilator needs, and deaths within US cities. Focusing on the Austin metropolitan area of Texas, we found that immediate and extensive social distancing measures were required to ensure that COVID-19 cases did not exceed local hospital capacity by early May 2020. School closures alone hardly changed the epidemic curve. A 2-week delay in implementation was projected to accelerate the timing of peak healthcare needs by 4 weeks and cause a bed shortage in intensive care units. This analysis informed the Stay Home-Work Safe order enacted by Austin on March 24, 2020.

Severe acute respiratory syndrome coronavirus 2 (SARS-CoV-2) appeared in Wuhan, China, during December 2019, and coronavirus disease (COVID-19) caused by this virus was declared a pandemic on March 11, 2020, by the World Health Organization (*1*). As of June 24, a total of 193 countries, areas, or territories had reported 9,129,146 confirmed COVID-19 cases and 473,797 deaths. Substantial outbreaks have occurred in India, Russia, Brazil, and the United States; the United States has the highest cumulative confirmed number of cases and deaths (*2*).

The United States reported its first imported SARS-CoV-2 case from Wuhan on January 20, in Washington (*3*), 6 days ahead of California (*4*) and 40 days ahead of New York, New York (*5*); the first locally infected cases were reported on February 28 (*6*). As of June 24, all 50 states had reported confirmed cases, 48 had reported community spread, and cumulative confirmed COVID-19 cases were 2,336,615 and deaths were 121,117 (*7*). Surges in COVID-19 hospitalizations have compromised local healthcare systems in New York (*8*) and Seattle (*9*).

Beginning in March 2020, states and cities implemented extensive social distancing measures to contain the spread of SARS-CoV-2, including school closures, limits on mass gatherings, shelter-in-place orders, travel restrictions, and bans on nonessential commercial activities. By early April, 45 states had issued a statewide shelter-in-place order or ≥1 city-level stay-at-home order, affecting >316 million persons. As of June 25, all measures have expired or relaxed (*10*). The timing of the orders varied; California was the first state to enact strict orders on March 19 and South Carolina the last on April 7 (*10*). These measures dramatically slowed the pace of the pandemic during April and May, but confirmed COVID-19 cases and hospitalizations have been increasing since early June, particularly in Arizona, Florida, Texas, and California (*11*).

As COVID-19 emerged into a global threat, we took a national pandemic influenza model that was built through a pandemic preparedness contract with the Centers for Disease Control and Prevention (CDC;

Author affiliations: The University of Texas at Austin, Austin, Texas, USA (X. Wang, R.F Pasco, Z. Du, M. Petty, S.J. Fox, L. Ancel Meyers); Yale University School of Public Health, New Haven, Connecticut, USA (A.P. Galvani); The University of Texas at Austin Dell Medical School, Austin (M. Pignone, S. Claiborne Johnston); Santa Fe Institute, Santa Fe, New Mexico, USA (L. Ancel Meyers)

DOI: https://doi.org/10.3201/eid2510.201702

[1]These authors contributed equally to this article.

Atlanta, GA, USA) and adapted it to model the spread and control of COVID-19 within and between 217 US cities. We used this model to project the potential effects of school closures coupled with social distancing, in terms of reducing cases, deaths, hospitalizations, intensive care unit (ICU) visits, and ventilator needs, on local, regional, and national scales. We have focused our analysis on Austin, which is the capital of Texas and the fastest growing city in the United States, as a representation of major US metropolitan areas. The scenarios and inputs (e.g., epidemiologic parameters) were determined in consultation with CDC and the Regional Healthcare System Executive Council of the Austin–Travis County Emergency Operations Command.

Methods

We focused on the Austin–Round Rock Statistical Metropolitan Area, which had a population of 2.17 million persons in 2018, but the qualitative findings and impact of social distancing will apply to cities throughout the United States. We analyzed a compartmental model that incorporates age-specific high risk proportions and contact rates to measure the effects of 2 key interventions, school closures and social distancing measures, which reduce nonhousehold contacts by a specified percentage. We estimated the effects of these measures on cases, hospitalizations, ICU visits, ventilator needs, and deaths.

We built a stochastic age- and risk-structured susceptible-exposed-asymptomatic-symptomatic-hospitalized-recovered (SEAYHR) model of SARS-CoV-2 transmission (Appendix Figure 1, https://wwwnc.cdc.gov/EID/article/26/10/20-1702-App1.pdf). Persons were separated into 5 age groups, <1–4, 5–17, 18–49, 50–64, and ≥65 years of age, on the basis of population data for the 5-county Austin–Round Rock Metropolitan Area from the 2017 American Community Survey (*12*). Each age group was divided into a low-risk and high-risk group on the basis of prevalence of chronic conditions estimated for the Austin population (Appendix Figure 2) (*13*–*16*). We also estimated the proportion of pregnant women in each age group as a special risk class (*17*). All persons were assumed to be susceptible to the disease. Infected persons were modeled to enter a latent period in which they were symptom-free and not yet infectious (*18*) and then progressed to either a symptomatic or asymptomatic compartment, both infectious. Asymptomatic persons were assumed to have the same infectious period as symptomatic persons but lower infectiousness. The rates at which symptomatic case-patients were moved to a hospitalized compartment and died depended on age and risk group. Recovered persons were considered fully immune. Deaths were assumed to occur after hospitalization. We provide a detailed description of the methods used (Appendix).

All model parameters (Appendix Tables 1–3) were based on published estimates from COVID-19 studies, as well as input from CDC and Austin. We assumed a basic reproduction number (R_0) of 2.2 (*19*) and considered 2 different doubling times, 7.2 days (low growth rate) (*19*–*21*) and 4 days (high growth rate) (*22*–*24*). We provide a sensitivity analysis for an R_0 of 3.5 (Appendix). Age-specific contact rates were estimated by using contact matrices published by Prem et al. and are adjusted to model school closures and various levels of social distancing (*25*). Transmission rates were estimated by fitting simulations to a given R_0 and epidemic doubling time. The latent period (i.e., noninfectious beginning of the incubation period) was sampled from a triangular distribution from 1.9 days to 3.9 days and a mean of 2.9 days (*26*,*27*), and the infectious period was sampled from a triangular distribution from 5.3 days to 7.3 days and a mean of 6.3 days (*27*). We assumed that 43% of infections are asymptomatic and that asymptomatic cases are two thirds as infectious as symptomatic cases (*28*,*29*). Following planning scenarios of CDC, we assumed that the infection hospitalization rate and infection fatality rate was 10 times higher in high-risk than low-risk persons within each age group.

Simulations began with 5 imported symptomatic cases in the 18–49-year-old age group on March 1, 2020, and were updated at 2.4-hour intervals. For each combination of epidemic scenarios (low/high growth rate) and intervention strategies (school closure policy with different levels of social distancing), we ran 100 stochastic simulations and reported the medians and 95% prediction intervals (ranges) at weekly intervals.

School Closure Policies

As part of a CDC modeling network, we initially modeled a large number of school closure policies, with variable implementation time and duration. To simulate school closures, we decreased the daily age-specific contact rates by the estimated number of contacts that occur within schools (*25*,*30*). The school-specific contact numbers encompass all interactions among students and teachers occurring at all educational levels, from elementary schools through colleges and universities. In our model, school closures reduced daily contacts by 15% for persons <1–4 years of age, 26% for persons 5–17 years of age, 9% for persons 18–49 of age, 9% for persons 50–64 of age, and 2% for

persons ≥64 years of age. We reported only 2 of these strategies to demonstrate the effects of implementation time: closure immediately after the first confirmed case (March 14) and delayed closure 2 months after the first confirmed case (May 14). In both cases, we assumed that schools remain closed through the end of the summer vacation (August 18, 2020), which corresponds to a 23-week duration for the early closure and a 14-week duration for the late closure. The early closure scenario roughly corresponded to Austin announcing the first 2 confirmed cases on March 13 and major school districts closing the next day. In our simulations, the median cumulative number of symptomatic COVID-19 cases by March 14th was 38 (interquartile range [IQR] 27–53) and 14 (IQR 9–19), assuming a 4-day and 7-day doubling period, respectively; by May 14, median cumulative symptomatic cases increased to 530,426 (IQR 114,151–783,667) and 3,206 (IQR 561–7,611), respectively.

Social Distancing Measures

In addition to school closures, we considered the effect of various levels of social distancing that decreased nonhousehold contacts by 25%, 50%, 75%, and 90% overall. These levels were chosen to correspond to increasingly more severe levels of restriction on social interaction from limiting large crowds to near-total restriction on out-of-home movement except for healthcare and basic necessities.

Age-stratified contact rates (*25*) were derived from the POLYMOD diary-based study in Europe (*30*) and separated in contacts occurring at home, at school, at work and elsewhere. We used the national US age distribution (*31*) to aggregate these estimates from 17 to the 5 age groups of our model (Appendix Tables 4–7). We combined these matrices to model 4 different types of days: normal school days (all contacts); normal weekends and short weekday holidays (all but school and work contacts; adults are assumed to work during the long summer break); weekdays during school closures/social distancing; and weekend or weekday holiday during school closure/social distancing. To model school closures with social distancing, we included all household contacts plus a specified proportion of contacts outside the home. On weekdays, this proportion included a proportion of contacts occurring at work and elsewhere; on weekends and holidays (excluding summer vacation), it included just contacts occurring elsewhere. Days were assigned to 1 of these 4 contact models on the basis of the 2019–2020 and 2020–2021 school calendars from the Austin Independent School District, which was the largest public school district in the metropolitan area, serving ≈22.7% of the Austin Round Rock Statistical Metropolitan Area population.

Healthcare Demands

We assumed that hospitalized cases were admitted on average 5.9 days (L. Tindale et al., unpub. data, https://doi.org/10.1101/2020.03.03.20029983) after symptom onset, with the infection hospitalization rate depending on the age and risk group (Appendix Table 1). Hospitalized case-patients who recovered were considered discharged an average of 11 days after admission; deaths occurred an average of 7.82 days after admission. We estimated the number ICU beds and ventilators needed to care for COVID-19 case-patients each day on the basis of age-specific rates provided by the CDC (Appendix Table 3) and assuming that the average duration of ICU care and ventilation support are 8 days and 5 days, respectively. There is some uncertainty regarding how these estimates might change when healthcare facilities reach or exceed capacity because of a lack of available postdischarge care and inefficiency in the healthcare system caused by worker illness. Thus, we also tested an alternative scenario with longer duration of hospital stay, ICU care, and ventilation (Appendix). We did not consider potential excess deaths resulting from lack of access to adequate healthcare during pandemic surges.

Results

Our analyses focus on 2 key levers of intervention: the speed of implementation and the extent of social distancing. We considered 2 scenarios for the epidemic growth rate of COVID-19 and project 5 outcomes: cases, hospitalizations, ICU care, ventilator needs, and deaths.

Regardless of epidemic growth rate, school closures alone had little effect on the burden of the epidemic. These closures would flatten the curve slightly if enacted immediately after the detection of the first case (Figure 1). High levels of social distancing, when coupled with school closures, substantially delayed and dampened the epidemic peak. The impact of the measures depended on early implementation. Under both the slower and faster epidemic growth scenarios (i.e., 7-day and 4-day doubling times), immediate measures beginning on March 14 were much more effective than 2-month delayed measures at slowing transmission throughout the spring and summer of 2020 (Figure 1). Given that recent estimates for the doubling time in US cities are short, ranging from 2.4 to 3 days (*24*,*32*), this finding suggests that proactive measures were justified, because delayed measures

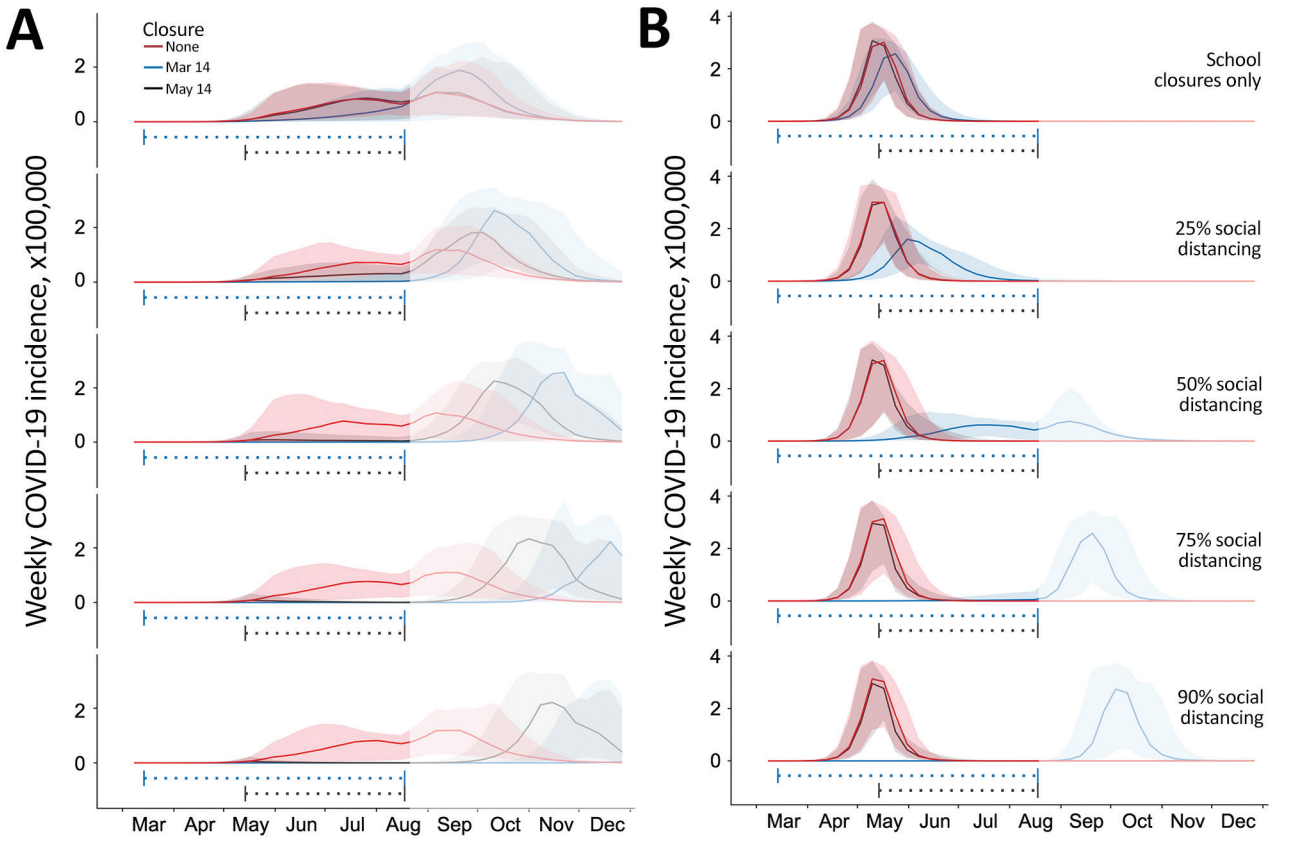

Figure 1. Projected weekly incident of COVID-19 cases in Austin–Round Rock Metropolitan Statistical Area, Texas, USA. Graphs show simulation results for different levels of social distancing and implementation times, assuming an epidemic doubling time of A) 7.2 days (*18–20,22*) or B) 4 days (*22–24*). Each graph displays 3 projections: a baseline assuming no social distancing (red), social distancing implemented March 14–Aug 17, 2020 (blue), and social distancing implemented May 14–Aug 17, 2020 (black). From top to bottom, the graphs in each column correspond to increasingly stringent social distancing measures: school closures plus social distancing that reduces nonhousehold contacts by 0%, 25%, 50%, 75%, or 90%. Solid lines indicate medians of 100 stochastic simulations; shading indicates inner 95% ranges of values. The horizontal dotted lines beneath the curves indicate intervention periods. The faded mid-August to December time range indicates long-range uncertainty regarding COVID-19 transmission dynamics and intervention policies. COVID-19, coronavirus disease.

would have been almost entirely ineffective. If the reproduction is higher than we assumed, then more vigilant social distancing would be required to slow spread (Appendix). Although the immediate school closure on March 14 had little impact on the initial wave, the August opening of schools would be expected to amplify a fall wave if the population is not yet close to herd immunity.

To assess the impact of social distancing measures on mitigating healthcare surge in the Austin–Round Rock Statistical Metropolitan Area, we considered the more plausible 4-day doubling time scenario (Table 1; Figure 2). Social distancing measures that reduced nonhousehold contacts by <50% were projected to delay but not prevent a healthcare crisis. Only the 75% and 90% contact reduction scenarios were projected to reduce hospitalizations, ICU care, and ventilator needs below the estimated capacity for the metropolitan area (Table 2). If 50% social distancing were implemented on March 28 instead of March 14 (i.e., a 2-week delay), we would expect COVID-19 ICU requirements to exceed local capacity by the end of June instead of only reaching capacity by the end of July (i.e., a 4-week acceleration) (Appendix). Under scenarios that predict overwhelming healthcare surges, we likely underestimate deaths because we do not account for excess deaths for persons with COVID-19 or other medical conditions, such as cancer or cardiovascular disease, who might not receive timely or safe care.

Under the naive scenario that school closures and social distancing measures are lifted entirely on the first day of the 2020–2021 academic year (August 18) (*33*), the pace and extent of COVID-19 transmission in the fall would depend on how many persons were infected (and thereby immunized)

Table 1. Estimated cumulative COVID-19 cases, healthcare requirements, and deaths, Austin–Round Rock metropolitan statistical area, Texas, USA, March 1–August 17, 2020*

Outcome	No measures	School closure	School closure and 50% social distancing	School closure and 75% social distancing	School closure and 90% social distancing
Cases	1,139,633 (1,092,754–1,173,408)	1,098,755 (1,016,794–1,143,147)	596,304 (215,897–854,094)	34,232 (2,871–244,959)	2,013 (642–11,358)
Hospitalizations	79,120 (75,373–82,608)	76,698 (70,091–80,602)	36,534 (11,474–57,912)	1,889 (159–13,512)	125 (32–660)
ICU	13,312 (12,673–13,890)	12,897 (11,786–13,540)	6141 (1,929–9,736)	318 (27–2,273)	21 (5–111)
Ventilators	6,274 (5,973–6,545)	6,077 (5,554–6,377)	2,893 (909–4,587)	150 (13–1,071)	10 (3–53)
Deaths	9,646 (9,031–10,206)	9,324 (8,481–9,954)	3,698 (995–6,751)	176 (13–1,315)	13 (1–70)

*Values are medians (95% prediction intervals) across 100 stochastic simulations based on parameters in Table 1. COVID-19, coronavirus disease; ICU, intensive care unit.

during the spring and summer (Figure 1). As cumulative incidence approaches the herd immunity threshold of roughly 55% of the population, the effective reproduction number (R_t) decreases. Once this 55% threshold is surpassed, the reproduction number decreases below 1, and the virus would be unable to spread widely, even if social distancing measures are lifted. Assuming the faster 4-day epidemic doubling time (Figure 1, panel B), a minimum of 50% social distancing is necessary to suppress transmission over the summer. Under 75% or 90% social distancing, the lifting of measures on August 18 would be expected to produce epidemic peaks in the middle or end of September, respectively. Assuming the slower 7-day doubling time (Figure 1, panel A), even delayed social distancing would be expected to forestall the start of the epidemic from spring to fall. The higher fall peaks that were produced under the most extreme social distancing, assuming a 7-day doubling time, stem from baseline contact patterns (in the absence of social distancing): a COVID-19 epidemic that begins in the spring would be naturally dampened by the 3-month summer vacation period when children are out of school, whereas a fall start would be amplified by the start of the academic year.

Discussion

As COVID-19 emerged as a global threat in early 2020, we rapidly adapted a pandemic influenza model that was under development as part of an effort coordinated by CDC to build a strategic national modeling resource for pandemic planning and response. The analyses provided in this report originated in time-sensitive requests from CDC, Austin, and the state of Texas to evaluate the potential impact of school closures and social distancing on the emergence and spread of COVID-19 in US cities. Our projections indicate that, without extensive social distancing measures, the emerging outbreak would quickly surpass healthcare capacity in the region. However, with extensive social distancing, the number of cases, hospitalizations, and deaths could be substantially reduced throughout the summer of 2020. Although these analyses are specific to the Austin–Round Rock metropolitan area, we expect that the impacts of the mitigation strategies will be qualitatively similar for cities throughout the United States.

Our epidemiologic projections and conclusions regarding the urgent need for extensive social distancing are consistent with a recent analysis by Imperial College London (*34*). However, we assume that a lower percentage of hospitalized patients receive critical care (15%–20% vs. 30%) and consequently project a lower peak ICU demand. In sensitivity analyses with more extreme assumptions about critical care requirements, the projected peak demand increases accordingly (Appendix). The local focus of our model, which incorporates city-specific data regarding demographics, high-risk conditions, contact patterns, and healthcare resource availability, enables us to project near-term healthcare demands and provide actionable insights for local healthcare and governmental decision-makers.

We conducted these analyses to inform decision making in a rapidly evolving environment with substantial uncertainty. On March 6, 2020, Austin declared a local state of disaster and cancelled the South by Southwest Conference and Festival, which was expected to draw 417,400 visitors from around the world and bring $355.9 million to the local economy (*35*). Evidence of community transmission appeared within days of the first confirmed COVID-19 case in Austin on March 13. Shortly after, the University of Texas at Austin, one of the largest public universities with >50,000 students, and the largest public school district in Austin announced school closures (*36*,*37*). On March 24, Austin issued a Stay Home-Work Safe order to eliminate all nonessential business and travels (*38*). Leaders of Austin requested the healthcare analyses (Figure 2) in the days leading up to the

order of March 24 and requested that we release a preliminary report to educate the public (*39*).

Social distancing measures, including school closures, restrictions on travel, mass gatherings and commercial activities, and more extensive shelter-in-place advisories, aim to decrease disease transmission within a population by preventing contacts between persons. Our analyses project the effect of such measures on the transmission dynamics of COVID-19 but do not consider the economic, social and psychological costs of social distancing measures, including the socioeconomic disparities in burden and illness and death resulting from reductions in health and mental healthcare services (*40*,*41*).

There is an urgent need to project the relative effects of different levels of social distancing in light of their potential societal costs, including school closures, partial work and travel restrictions and cocooning of the high risk, so that restrictions can be strategically lifted without compromising public health. In particular, school closures are often deployed earlier than more extensive social distancing measures. However, such closures can be costly, particularly for low-income families who might rely on lunch programs and be unable to afford childcare (*42*,*43*), and our analysis suggests that they might only slightly reduce the pace of transmission and peak hospital surge. However, the role of children in community transmission of COVID-19 remains uncertain; thus, school closures are prudent at this time. Children represent a low proportion of confirmed cases worldwide (*44*,*45*), perhaps reflecting that COVID-19 is less severe in children than adults (*46*). If we learn that the prevalence or infectiousness of COVID-19 is low in children, then opening schools may be a reasonable first step toward resuming normalcy.

Although our model incorporates considerable detail regarding the natural history of COVID-19, age- and location-specific contact patterns, and the demographic and risk composition of the Austin–Round Rock Statistical Metropolitan Area, it does

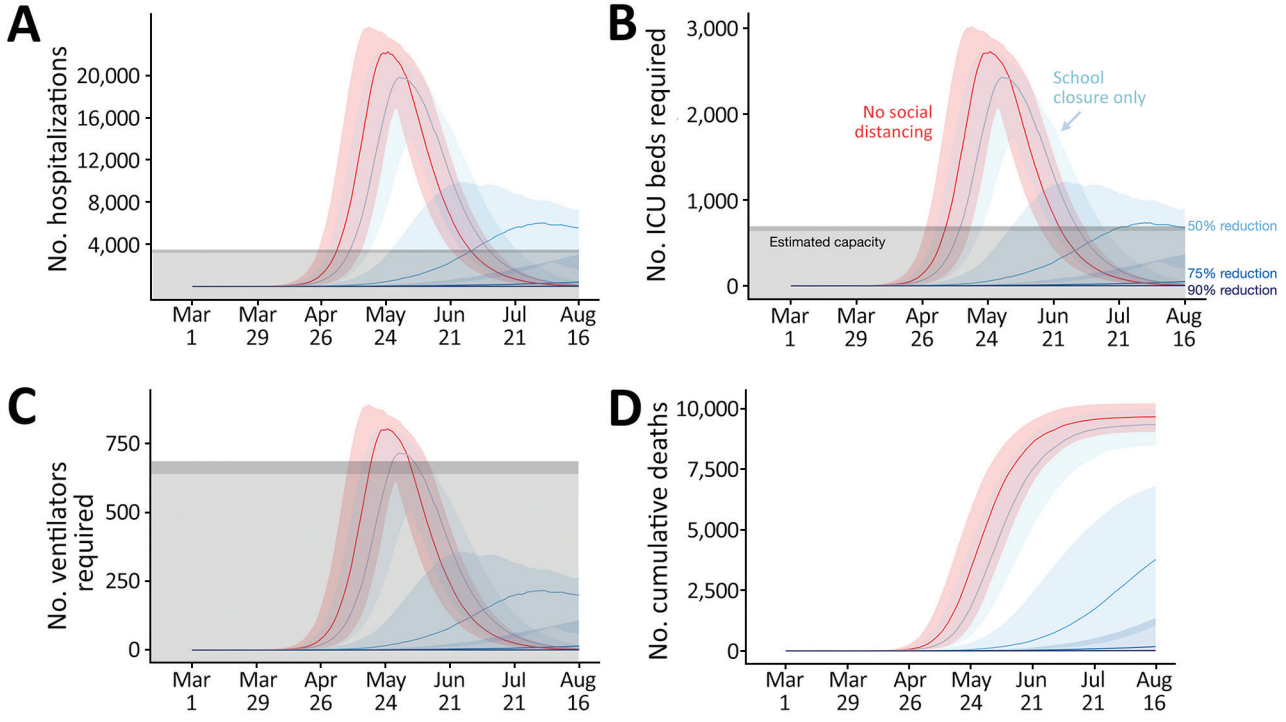

Figure 2. Projected COVID-19 healthcare demand and cumulative deaths in Austin–Round Rock Metropolitan Statistical Area, Texas, USA. Graphs show simulation results across multiple levels of social distancing, assuming a basic reproductive number of 2.2 with a 4-day epidemic doubling time. Extensive social distancing is expected to substantially reduce the burden of COVID-19 A) hospitalizations, B) patients requiring ICU care, C) patients requiring mechanical ventilation, and D) cumulative deaths. Red lines indicate projected COVID-19 transmission assuming no interventions under the parameters given in Table A1. Blue lines indicate increasing levels of social distancing interventions, from light to dark: school closures plus social distancing interventions that reduce nonhousehold contacts by either 0%, 50%, 75%, or 90%. Lines and shading indicate medians and inner 95% ranges of values across 100 stochastic simulations. Gray shaded region indicates estimated surge capacity for COVID-19 patients in the Austin-Round Rock Metropolitan Statistical Area as of March 28, 2020, which is calculated on the basis of 80% of the total 4,299 hospital beds, 90% of the total 755 ICU beds, and 755 mechanical ventilators. COVID-19, coronavirus disease; ICU, intensive care unit.

Table 2. Estimated peak COVID-19 cases and healthcare demands, Austin–Round Rock metropolitan statistical area, Texas, USA, March 1–August 17, 2020*

Outcome	No measures	School closure	School closure and 50% social distancing	School closure and 75% social distancing	School closure and 90% social distancing
Cases	272,978 (228,088–327,181)	237,428 (176,910–281,441)	64,779 (33,837–110,968)	4,643 (267–35,148)	163 (42–1,279)
New cases daily	54,106 (47,301–62,646)	43,535 (33,691–50,105)	10,573 (6,297–16,768)	851 (57–5,436)	32 (10–212)
Hospitalizations	23,073 (20,961–24,695)	20,671 (17,193–22,473)	6,804 (3,088–10,271)	402 (31–2,963)	18 (5–105)
ICU	2,831 (2,575–3,033)	2,532 (2,107–2,759)	833 (377–1,254)	50 (4–362)	2 (1–13)
Ventilators	835 (760–895)	746 (621–814)	245 (111–369)	15 (1–107)	1 (0–4)

*Values are medians (95% prediction intervals) across 100 stochastic simulations based on parameters in Table 1. COVID-19, coronavirus disease; ICU, intensive care unit.

not explicitly capture neighborhood, household, or other community structure that can serve to amplify or impede transmission (*47*–*49*). In addition, we ignored the possible importation of COVID-19 cases from other cities, under the assumption that the additional cases would have a negligible impact, particularly during the period of exponential growth. Although large numbers of introductions could undermine mitigation efforts that radically suppress transmission, we conjecture that such efforts would include travel restrictions, contact tracing and other measures to contain emerging clusters. Our model also does not evaluate other potentially effective interventions, such as increased levels of selective testing and isolation.

These analyses rely on recently published estimates for transmission rate and severity of COVID-19, as well as best estimates from expert opinions from CDC and Dell Medical School. There is still much we do not understand about the transmission dynamics of SARS-CoV-2, including its R_0, the infectiousness of asymptomatic case-patients (*28*), and the extent to which infections confer future immunity (*50*), all of which are key to anticipating future pandemic waves. As of June 2020, it is likely most US cities remain far from herd immunity. Even in New York, New York, which experienced a substantially larger first wave than other cities, serologic surveys suggest that only 22.7% of the population has been exposed (E.S. Rosenberg et al., unpub. data, https://doi.org/10.1101/2020.05.25.20113050). However, summer surges in transmission in some cities might infect large numbers of persons by the beginning of the fall semester. In that case, resolving these key uncertainties will be critical to projecting the full impact of school openings. Our understanding of COVID-19 is evolving so rapidly that we expect there might be consensus around different estimates for key transmission and severity parameters by the time this work is published. Thus, we emphasize the qualitative but not quantitative results of the analysis.

Given the rapid spread of COVID-19, early and extensive social distancing are both viable and necessary for preventing catastrophic hospital surges. Despite this study's uncertainties in key parameters and the focus on a single city, the expansion and containment of COVID-19 in cities worldwide suggest that these insights are widely applicable. This framework can be updated as situational awareness of COVID-19 improves to provide a quantitative sounding board as public health agencies evaluate strategies for mitigating risks while sustaining economic activity in the United States.

Acknowledgments

We thank Matthew Biggerstaff, Michael Johannson, the FluCode network at CDC, Steven Adler, and the White House Coronavirus Task Force for providing critical discussions and parameter guidance

About the Author

Ms. Wang is a PhD candidate at the University of Texas at Austin. Her primary research interest is mathematical and statistical modeling of infectious disease dynamics.

References

1. The Washington Post. WHO declares a pandemic of coronavirus disease COVID-19, 2020 Mar 11 [cited 2020 Mar 25]. https://www.washingtonpost.com/health/2020/03/11/who-declares-pandemic-coronavirus-disease-covid-19
2. World Health Organization. Novel coronavirus (2019-nCoV) situation reports [cited 2020 Mar 30]. https://www.who.int/emergencies/diseases/novel-coronavirus-2019/situation-reports
3. Holshue ML, DeBolt C, Lindquist S, Lofy KH, Wiesman J, Bruce H, et al.; Washington State 2019-nCoV Case Investigation Team. First case of 2019 novel coronavirus in the United States. N Engl J Med. 2020;382:929–36. https://doi.org/10.1056/NEJMoa2001191
4. Wheeler I. Orange County coronavirus patient released, in good condition, health officials say. Orange County Register. Orange County Register. 2020 Feb 4 [cited 2020 Mar 26]. https://www.ocregister.com/risk-of-catching-coronavirus-in-so-cal-is-low-health-officials-say

5. Goldstein J, McKinley J. Second case of coronavirus in N.Y. sets off search for others exposed. The New York Times. 2020 Mar 3 [cited 2020 Mar 26]. https://www.nytimes.com/2020/03/03/nyregion/coronavirus-new-york-state.html
6. Centers for Disease Control and Prevention. Coronavirus 2019; 2020 [cited 2020 Mar 25]. https://www.cdc.gov/media/releases/2020/t0228-COVID-19-update.html
7. Centers for Disease Control and Prevention. Coronavirus disease 2019 (COVID-19) in the US; 2020 [cited 2020 Mar 25]. https://www.cdc.gov/coronavirus/2019-ncov/cases-updates/cases-in-us.html
8. Koenig D. NYC hospitals struggle with coronavirus surge. WebMD. 2020 [cited 2020 Mar 28]. https://www.webmd.com/lung/news/20200326/nyc-hospitals-struggle-with-coronavirus-surge
9. Bush E, Gilbert D. Short-staffed and undersupplied: coronavirus crisis strains Seattle area's capacity to deliver care. The Seattle Times. 2020 Mar 12 [cited 2020 Mar 28]. https://www.seattletimes.com/seattle-news/health/short-staffed-and-undersupplied-coronavirus-crisis-strains-seattle-areas-capacity-to-deliver-care
10. Mervosh S, Lu D, Swales V. See which states and cities have told residents to stay at home. The New York Times, 2020 Mar 24 [cited 2020 Mar 28]. https://www.nytimes.com/interactive/2020/us/coronavirus-stay-at-home-order.html
11. Adeline S, Jin CH, Hurt A, Wilburn T, Wood D, Talbot R. Tracking the pandemic: are coronavirus cases rising or falling in your state? NPR. 2020 Jun 25 [cited 2020 Jun 25]. https://www.npr.org/sections/health-shots/2020/03/16/816707182/map-tracking-the-spread-of-the-coronavirus-in-the-u-s
12. US Census Bureau. American Community Survey (ACS) [cited 2019 Nov 19]. https://www.census.gov/programs-surveys/acs
13. Centers for Disease Control and Prevention. 500 cities project: Local data for better health; 2019 [cited 2020 Mar 19]. https://www.cdc.gov/500cities/index.htm
14. Centers for Disease Control and Prevention. HIV surveillance report, 2016. 2017 Nov [cited 2020 Jul 8]. https://www.cdc.gov/hiv/library/reports/hiv-surveillance.html
15. Morgan OW, Bramley A, Fowlkes A, Freedman DS, Taylor TH, Gargiullo P, et al. Morbid obesity as a risk factor for hospitalization and death due to 2009 pandemic influenza A(H1N1) disease. [Internet]. PLoS One. 2010;5:e9694. https://doi.org/10.1371/journal.pone.0009694
16. Sturm R, Hattori A. Morbid obesity rates continue to rise rapidly in the United States. Int J Obes. 2013;37:889–91. https://doi.org/10.1038/ijo.2012.159
17. Centers for Disease Control and Prevention. Estimating the number of pregnant women in a geographic area. Division of Reproductive Health [cited 2020 Jul 8]. https://www.cdc.gov/reproductivehealth/emergency/pdfs/PregnacyEstimatoBrochure508.pdf
18. Du Z, Xu X, Wu Y, Wang L, Cowling BJ, Meyers LA. Serial interval of COVID-19 among publicly reported confirmed cases. Emerg Infect Dis. 2020;26:1341–3. https://doi.org/10.3201/eid2606.200357
19. Li Q, Guan X, Wu P, Wang X, Zhou L, Tong Y, et al. Early transmission dynamics in Wuhan, China, of novel coronavirus-infected pneumonia. N Engl J Med. 2020;382:1199–207. https://doi.org/10.1056/NEJMoa2001316
20. Wu JT, Leung K, Leung GM. Nowcasting and forecasting the potential domestic and international spread of the 2019-nCoV outbreak originating in Wuhan, China: a modelling study. Lancet. 2020;395:689–97. https://doi.org/10.1016/S0140-6736(20)30260-9
21. Du Z, Wang L, Cauchemez S, Xu X, Wang X, Cowling BJ, et al. Risk for transportation of coronavirus disease from Wuhan to other cities in China. Emerg Infect Dis. 2020;26:1049–52. https://doi.org/10.3201/eid2605.200146
22. Kraemer MU, Yang C-H, Gutierrez B, Wu C-H, Klein B, Pigott DM, et al.; Open COVID-19 Data Working Group. The effect of human mobility and control measures on the COVID-19 epidemic in China. Science. 2020;368:493–7. https://doi.org/10.1126/science.abb4218
23. Muniz-Rodriguez K, Chowell G, Cheung C-H, Jia D, Lai P-Y, Lee Y, et al. Doubling time of the COVID-19 epidemic by province, China. Emerg Infect Dis. 2020;26: August; Epub ahead of print. https://doi.org/10.3201/eid2608.200219
24. Roser M, Ritchie H, Ortiz-Ospina E. Coronavirus disease (COVID-19): statistics and research. Our world in data, 2020 [cited 2020 Jul 8]. https://ourworldindata.org/coronavirus?fbclid=IwAR2qRdLFRmugoD0w_r13O4HAOHrL1hiHfduyB2XvtXNjtQ5GGW6Dg9EsIZA
25. Prem K, Cook AR, Jit M. Projecting social contact matrices in 152 countries using contact surveys and demographic data. PLOS Comput Biol. 2017;13:e1005697. https://doi.org/10.1371/journal.pcbi.1005697
26. Zhang J, Litvinova M, Wang W, Wang Y, Deng X, Chen X, et al. Evolving epidemiology and transmission dynamics of coronavirus disease 2019 outside Hubei province, China: a descriptive and modelling study. Lancet Infect Dis. 2020;20:793–802. https://doi.org/10.1016/S1473-3099(20)30230-9
27. He X, Lau EH, Wu P, Deng X, Wang J, Hao X, et al. Temporal dynamics in viral shedding and transmissibility of COVID-19. Nat Med. 2020;26:672–5. https://doi.org/10.1038/s41591-020-0869-5
28. He D, Zhao S, Lin Q, Zhuang Z, Cao P, Wang MH, et al. The relative transmissibility of asymptomatic COVID-19 infections among close contacts. Int J Infect Dis. 2020;94: 145–7. https://doi.org/10.1016/j.ijid.2020.04.034
29. Gudbjartsson DF, Helgason A, Jonsson H, Magnusson OT, Melsted P, Norddahl GL, et al. Spread of SARS-CoV-2 in the Icelandic population. N Engl J Med. 2020;382:2302–15. https://doi.org/10.1056/NEJMoa2006100
30. Mossong J, Hens N, Jit M, Beutels P, Auranen K, Mikolajczyk R, et al. Social contacts and mixing patterns relevant to the spread of infectious diseases. PLoS Med. 2008;5:e74. https://doi.org/10.1371/journal.pmed.0050074
31. United Nations. Record view: population by age, sex and urban/rural residence [cited 2020 Mar 22]. http://data.un.org/Data.aspx?d=POP&f=tableCode%3a22
32. Siegel E. Why "exponential growth" is so scary for the COVID-19 coronavirus. Forbes Magazine, 2020 Mar 17 [cited 2020 Mar 30]. https://www.forbes.com/sites/startswithabang/2020/03/17/why-exponential-growth-is-so-scary-for-the-covid-19-coronavirus
33. Austin Independent School District. Calendar of events, 2020 [cited 2020 Mar 26]. https://www.austinisd.org/calendar
34. Ferguson NM, Laydon D, Nedjati-Gilani G, Imai N, Ainslie K, Baguelin M, et al. Impact of non-pharmaceutical interventions (NPIs) to reduce COVID-19 mortality and healthcare demand, 2020. Imperial College London. 2020 [cited 2020 Jul 8]. https://sciencebusiness.net/sites/default/files/inline-files/Imperial-College-COVID19-NPI-modelling-16-03-2020.pdf
35. SXSW. Facts, figures & quotes. SXSW Conference & Festivals [cited 2020 Mar 25]. https://www.sxsw.com/facts-figures-quotes

36. Austin Independent School District. Important message. 2020 Mar 13 [cited 2020 Mar 26]. https://www.austinisd.org/announcements/2020/03/13/important-message-mensaje-importante
37. The University of Texas at Austin. COVID-19 updates. Guidance related to the coronavirus disease, 2020 [cited 2020 Mar 26]. https://coronavirus.utexas.edu/all-campus-communications-covid-19
38. City of Austin, Texas. Coronavirus disease. 2019 (COVID-19) [cited 2020 Mar 25]. http://www.austintexas.gov/COVID19
39. University of Texas News. A new Texas COVID-19 pandemic toolkit shows the importance of social distancing. 2020 Mar 26 [cited 2020 Mar 28]. https://news.utexas.edu/2020/03/26/a-new-texas-covid-19-pandemic-toolkit-shows-the-importance-of-social-distancing
40. Chen Q, Liang M, Li Y, Guo J, Fei D, Wang L, et al. Mental health care for medical staff in China during the COVID-19 outbreak. Lancet Psychiatry. 2020;7:e15–6. https://doi.org/10.1016/S2215-0366(20)30078-X
41. Maharaj S, Kleczkowski A. Controlling epidemic spread by social distancing: do it well or not at all. BMC Public Health. 2012;12:679. https://doi.org/10.1186/1471-2458-12-679
42. Lempel H, Epstein JM, Hammond RA. Economic cost and health care workforce effects of school closures in the U.S. PLoS Curr. 2009;1:RRN1051. https://doi.org/10.1371/currents.RRN1051
43. Araz OM, Damien P, Paltiel DA, Burke S, van de Geijn B, Galvani A, et al. Simulating school closure policies for cost effective pandemic decision making. BMC Public Health. 2012;12:449. https://doi.org/10.1186/1471-2458-12-449
44. Guan W-J, Ni Z-Y, Hu Y, Liang W-H, Ou C-Q, He J-X, et al.; China Medical Treatment Expert Group for Covid-19. Clinical characteristics of coronavirus disease 2019 in China. N Engl J Med. 2020;382:1708–20. https://doi.org/10.1056/NEJMoa2002032
45. Verity R, Okell LC, Dorigatti I, Winskill P, Whittaker C, Imai N, et al. Estimates of the severity of coronavirus disease 2019: a model-based analysis. Lancet Infect Dis. 2020;20:669–77. https://doi.org/10.1016/S1473-3099(20)30243-7
46. Liu W, Zhang Q, Chen J, Xiang R, Song H, Shu S, et al. Detection of COVID-19 in children in early January 2020 in Wuhan, China. N Engl J Med. 2020;382:1370–1. https://doi.org/10.1056/NEJMc2003717
47. Hoen AG, Hladish TJ, Eggo RM, Lenczner M, Brownstein JS, Meyers LA. Epidemic wave dynamics attributable to urban community structure: a theoretical characterization of disease transmission in a large network. J Med Internet Res. 2015;17:e169. https://doi.org/10.2196/jmir.3720
48. Meyers LA, Pourbohloul B, Newman ME, Skowronski DM, Brunham RC. Network theory and SARS: predicting outbreak diversity. J Theor Biol. 2005;232:71–81. https://doi.org/10.1016/j.jtbi.2004.07.026
49. Volz EM, Miller JC, Galvani A, Ancel Meyers L. Effects of heterogeneous and clustered contact patterns on infectious disease dynamics. PLOS Comput Biol. 2011;7:e1002042. https://doi.org/10.1371/journal.pcbi.1002042
50. Long Q-X, Tang X-J, Shi Q-L, Li Q, Deng H-J, Yuan J, et al. Clinical and immunological assessment of asymptomatic SARS-CoV-2 infections. Nat Med. 2020;Jun 18 {Epub ahead of print].. https://doi.org/10.1038/s41591-020-0965-6

Address for correspondence: Lauren Ancel Meyers, Department of Integrative Biology, The University of Texas at Austin, 1 University Station C0990, Austin, TX 78712, USA; email: laurenmeyers@austin.utexas.edu

Article DOI: https://doi.org/10.3201/eid2510.201702

Impact of Social Distancing Measures on Coronavirus Disease Healthcare Demand, Central Texas, USA

Appendix.

Section 1. COVID-19 Epidemic Model Structure and Parameters

The model structure is diagrammed in Appendix Figure 1 and described in the equations below.

For each age and risk group, we build a separate set of compartments to model the transitions between the states: susceptible (*S*), exposed (*E*), symptomatic infectious (I^Y), asymptomatic infectious (I^A), symptomatic infectious that are hospitalized (I^H), recovered (*R*), and deceased (*D*). The symbols *S*, *E*, I^Y, I^A, I^H, *R*, and *D* denote the number of people in that state in the given age/risk group and the total size of the age/risk group is $N = S + E + I^Y + I^A + I^H + R + D$.

The model for individuals in age group *a* and risk group *r* is given by:

$$\frac{dS_{a,r}}{dt} = -\sum_{i\in A}\sum_{j\in K}\left(I^Y_{i,j}\omega^Y + I^A_{i,j}\omega^A + E_{i,j}\omega^E\right)\beta\phi_{a,i}/N_i$$

$$\frac{dE_{a,r}}{dt} = \sum_{i\in A}\sum_{j\in K}\left(I^Y_{i,j}\omega^Y + I^A_{i,j}\omega^A + E_{i,j}\omega^E\right)\beta\phi_{a,i}/N_i - \sigma E_{a,r}$$

$$\frac{dI^A_{a,r}}{dt} = (1-\tau)\,\sigma E_{a,r} - \gamma^A I^A_{a,r}$$

$$\frac{dI^Y_{a,r}}{dt} = \tau\sigma E_{a,r} - (1-\pi)\,\gamma^Y I^Y_{a,r} - \pi\eta I^Y_{a,r}$$

$$\frac{dI^H_{a,r}}{dt} = \pi\eta I^Y_{a,r} - (1-\nu)\,\gamma^H I^H_{a,r} - \nu\mu I^H_{a,r}$$

$$\frac{dR_{a,r}}{dt} = \gamma^A I^A_{a,r} + (1-\pi)\,\gamma^Y I^Y_{a,r} + (1-\nu)\,\gamma^H I^H_{a,r}$$

$$\frac{dD_{a,r}}{dt} = \nu\mu I^H_{a,r}$$

where A and K are all possible age and risk groups, ω^A, ω^Y , ω^H are relative infectiousness of the I^A, I^Y , E compartments, respectively, β is transmission rate, $\phi_{a,i}$ is the mixing rate between age group a, $i \in A$, γ^A,γ^Y , γ^H are the recovery rates for the I^A, I^Y , I^H compartments, respectively, σ is the exposed rate, τ is the symptomatic ratio, π is the proportion of symptomatic individuals requiring hospitalization, η is rate at which hospitalized cases enter the hospital following symptom onset, ν is mortality rate for hospitalized cases, and μ is rate at which terminal patients die.

Initial conditions, school closures and social distancing policies are shown in Appendix Table 1. We model stochastic transitions between compartments using the τ-leap method (*1*,*2*) with key parameters given in Appendix Table 2. Hospitalization parameters are shown in Appendix Table 3. Assuming that the events at each time-step are independent and do not impact the underlying transition rates, the numbers of each type of event should follow Poisson distributions with means equal to the rate parameters. We thus simulate the model according to the following equations:

$$S_{a,r}(t+1) - S_{a,r}(t) = -P_1$$

$$E_{a,r}(t+1) - E_{a,r}(t) = P_1 - P_2$$

$$IaA,r(t+1) - IaA,r(t) = (1-\tau)P_2 - P_3$$

$$IaY,r(t+1) - IaY,r(t) = \tau P_2 - P_4 - P_5$$

$$IaH,r(t+1) - IaH,r(t) = P_5 - P_6 - P_7$$

$$R_{a,r}(t+1) - R_{a,r}(t) = P_3 + P_4 + P_6$$

$$D_{a,r}(t+1) - D_{a,r}(t) = P_7,$$

with

$$P_1 \sim Pois(S_{a,r}(t)F_{a,r}(t))$$

$$P_2 \sim Pois(\sigma E_{a,r}(t))$$

$$P_3 \sim Pois(\gamma^A I_a{}^A{}_{,r}(t))$$

$$P_4 \sim Pois((1-\pi)\gamma^Y I_a{}^Y{}_{,r}(t))$$

$$P_5 \sim Pois(\pi\eta I_a{}^Y{}_{,r}(t))$$

$$P_6 \sim Pois((1-\nu)\gamma^H I_a{}^H)$$

$P_7 \sim Pois(\nu\mu I_a^H{}_{,r}(t))$

and where $F_{a,r}$ denotes the force of infection for individuals in age group a and risk group r and is given by:

$$F_{a,r}(t) = \sum_{i \in A} \sum_{j \in K} \left(I_{i,j}^{Y}(t)\omega^{Y} + I_{i,j}^{A}(t)\omega^{A} + E_{i,j}(t)\omega^{E} \right) \beta_{a,i}\Phi_{a,i}/N_i \, .$$

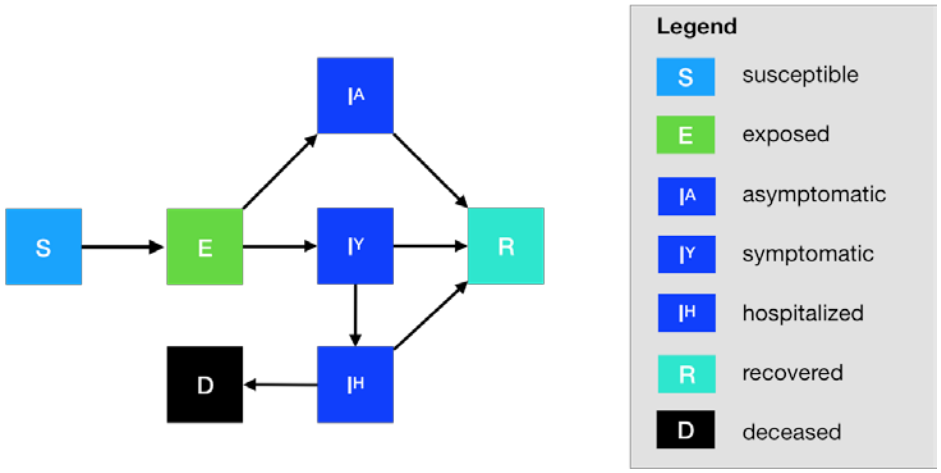

Appendix Figure 1. Compartmental model of COVID-19 transmission in a US city. Each subgroup **(**defined by age and risk) is modeled with a separate set of compartments. Upon infection, susceptible individuals (*S*) progress to exposed (*E*) and then to either symptomatic infectious (I^Y) or asymptomatic infectious (*IA*). All asymptomatic cases eventually progress to a recovered class where they remain protected from future infection (*R*); symptomatic cases are either hospitalized (*I*) or recover. Mortality (*D*) varies by age group and risk group and is assumed to be preceded by hospitalization.

Appendix Table 1. Initial conditions, school closures and social distancing policies

Variable	Settings
Initial day of simulation	3/1/2020
Initial infection number in locations	5 symptomatic cases in 18–49y age group
Trigger to close school	3/14/2020
Closure Duration	Until start of 2020–2021 school year (8/17/20)
α: Reduction of nonhousehold contacts (work and other)	Five scenarios: 0, 0.25, 0.5, 0.75, 0.9
Age-specific and day-specific contact rates	Home, work, other and school matrices provided in Appendix Tables 4–7; Normal weekday = home + work + other + school; Normal weekend = home + other; Normal weekday holiday = home + other; Normal weekday during summer or winter break = home + work + other; School closure weekday = home + (1 – α) × (work + other); School closure weekend = home + (1 – α) × (other); School closure weekday holiday = home + (1 – α) × (other); School closure during summer or winter break = home + (1 – α) × (work + other)

Appendix Table 2. Model parameters in which values that are given as 5element vectors are age-stratified with values corresponding to 0–4, 5–17, 18–49, 50–64, 65+ year age groups, respectively*

Parameter	Best guess – values (doubling time = 7.2 d)	Best guess values (doubling time = 4 d)	Source
R0	2.2	2.2	Li et al. (*3*)
δ: doubling time	7.2 d	4 d	Kraemer et al. (*4*)
β: transmission rate*	0.0311915	0.0500845	Fitted[a] to obtain specified *R0* given δ
γ^A : recovery rate on asymptomatic infectious compartment	Equal to γ^Y		
γ^Y: recovery rate on symptomatic infectious nontreated compartment	$\frac{1}{Y}$ ~ *Triangular* (5.3, 6.3, 7.3) γ		(*5*)
τ: symptomatic proportion (%)	57		(*6*)
σ: exposed rate	$\frac{1}{}$ ~ *Triangular* (1.9, 2.9, 3.9) σ		Based on incubation (*7*) and presymptomatic periods (*5*)
ω^E: relative infectiousness of individuals in compartment E	$\omega^E = 0$		
ω^A : relative infectiousness of infectious individuals in compartment I^A	2.3		He et al. (*8*)
IFR: infected fatality ratio, age specific (%)	Overall: [0.0016, 0.0049, 0.084, 1.000, 3.371]; Low risk: [0.00091668, 0.0021789, 0.03388, 0.25197, 0.64402]; High risk: [0.009167, 0.02179, 0.33878, 2.5197, 6.4402]		Age adjusted from Verity et al. (*9*)
YFR: symptomatic fatality ratio, age specific (%)	Overall: [0.002807, 0.008678, 0.1479, 1.755, 5.915]; Low risk: [0.001608, 0.003823, 0.05943,0.4420, 1.130]; High risk: [0.01608, 0.03823, 0.5943, 4.420, 11.30]		*Y FR* = *IF*τ*R*
h: high-risk proportion, age specific (%)	[8.2825, 14.1121, 16.5298, 32.9912, 47.0568]		Estimated using 2015–2016; Behavioral Risk Factor; Surveillance System (BRFSS) data with multilevel regression and poststratification using CDC's list of conditions that might increase the risk of serious complications from influenza (*10–12*)
rr: relative risk for high-risk persons compared with low risk in their age group	10		Assumption
School calendars	Austin Independent School District calendar (2019–2020, 2020–2021)		(*13*)

*The parameter β is fitted through constrained trust-region optimization in SciPy/Python (14). Given a value of β, a deterministic simulation is run based on central values for each parameter, from which we can compute the implied R_0 (β). We (*1*) track the daily number of new cases I_t (both symptomatic and asymptomatic) during the exponential growth portion of the epidemic (*2*), compute the log of the number of new cases: $y_t = log\ (I_t)$ and (*3*) use least squares to fit a line to this curve: $\log(I_t) = y_0 + g \times t$. We then estimate the reproduction number R_0 (β) of the simulation for that specific value of β as R_0 (β) = $1 \Gamma + g \times 1$ where Γ is the generation time given by $\Gamma = \delta(R_0 - 1)/\log(2)$. The optimizing function runs until the resulting value of R_0 (β) does not get closer to the target value.

We (*1*) track the daily number of new cases I_t (both symptomatic and asymptomatic) during the exponential growth portion of the epidemic (*2*), compute the log of the number of new cases: $y_t = log\ (I_t)$ and (*3*) use least squares to fit a line to this curve: $log^{(I_t)} = y_0 + g \cdot t$. We then estimate the reproduction number R_0 (β) of the $\delta(R^0-1)$ simulation for that specific value of β as $R_0(\beta) = \Gamma \cdot g + 1$ where Γis the generation time given by $\Gamma = \frac{}{log\ (2)}$.

The optimizing function runs until the resulting value of R_0 (β) does not get closer to the target value.

Appendix Table 3. Hospitalization parameters

Parameter	Value	Source
γ^H : recovery rate in hospitalized compartment	0.0912409	10.96 d-average from admission to discharge (Fit to Austin admissions and discharge data)
YHR: symptomatic case hospitalization rate (%)	Overall: [0.07018, 0.07018, 4.735, 16.33, 25.54]; Low risk: [0.04021, 0.03091, 1.903, 4.114, 4.879]; High risk: [0.4021, 0.3091, 19.03, 41.14, 48.79]	Age adjusted from Verity et al. (9)
π: rate of symptomatic individuals go to hospital, age-specific	$\pi = \frac{\gamma^Y \cdot YHR}{\eta+(\gamma^Y-\eta)YHR}$	
η: rate from symptom onset to hospitalized	0.12195	5.9 d average from symptom onset to hospital admission (L. Tindale et al., unpub. data, https://doi.org/10.1101/2020.03.03.20029983) and 2.3 d pre-symptomatic period from He et al. (5)
μ: rate from hospitalized to death	0.12821	7.8 d-average from admission to death (Fit to Austin admissions and discharge data)
HFR: hospitalized fatality ratio, age specific (%)	[4, 12.365, 3.122, 10.745, 23.158]	$HFR = \frac{YFR}{YHR}$
ν: death rate on hospitalized individuals age specific	[0.0390, 0.1208, 0.0304, 0.1049, 0.2269]	$\nu = \frac{\gamma^H HFR}{\mu+(\gamma^H-\mu)HFR}$
ICU: proportion hospitalized people in ICU	[0.15, 0.20, 0.15, 0.20, 0.15]	CDC COVID-19 planning scenarios (based on US seasonal flu data)
Vent: proportion of individuals in ICU needing ventilation	[0.35, 0.3, 0.45, 0.5, 0.45]	CDC planning scenarios (based on US seasonal flu data)
d_{ICU} : duration of stay in ICU	8 d	Assumption, computed as average of hospital stay and ventilation durations
d_V : duration of ventilation	5 d	CDC COVID-19 planning scenarios
HCS:healthcare capacity	Hospital bed: 4,299; ICU bed: 755; Ventilator: 755	Estimates provided by each of the region's hospital systems and aggregated by regional public health leaders

Appendix Table 4. Home contact matrix (daily number contacts by age group at home)

Age, y	0–4	5–17	18–49	50–64	≥65
<1–4	0.5	0.9	2.0	0.1	0.0
5–17	0.2	1.7	1.9	0.2	0.0
18–49	0.2	0.9	1.7	0.2	0.0
50–64	0.2	0.7	1.2	1.0	0.1
≥65	0.1	0.7	1.0	0.3	0.6

Appendix Table 5. School contact matrix (daily number contacts by age group at school)

Age, y	0–4	5–17	18–49	50–64	≥65
<1–4	1.0	0.5	0.4	0.1	0.0
5–17	0.2	3.7	0.9	0.1	0.0
18–49	0.0	0.7	0.8	0.0	0.0
50–64	0.1	0.8	0.5	0.1	0.0
≥65	0.0	0.0	0.1	0.0	0.0

Appendix Table 6. Work contact matrix (daily number contacts by age group at work)

Age, y	0–4	5–17	18–49	50–64	≥65
>1–4	0.0	0.0	0.0	0.0	0.0
5–17	0.0	0.1	0.4	0.0	0.0
18–49	0.0	0.2	4.5	0.8	0.0
50–64	0.0	0.1	2.8	0.9	0.0
≥65	0.0	0.0	0.1	0.0	0.0

Appendix Table 7. Others contact matrix (daily number contacts by age group at other locations)

Age, y	0–4	5–17	18–49	50–64	≥65
>1–4	0.7	0.7	1.8	0.6	0.3
5–17	0.2	2.6	2.1	0.4	0.2
18–49	0.1	0.7	3.3	0.6	0.2
50–64	0.1	0.3	2.2	1.1	0.4
≥65	0.0	0.2	1.3	0.8	0.6

Section 2. Estimation of age-stratified proportion of population at high risk for COVID-19 complications

High-risk conditions for influenza and data sources for prevalence estimation are shown in Appendix Table 8. We estimate age-specific proportions of the population at high risk of complications from COVID-19 based on data for Austin, TX and Round-Rock, TX from the CDC's 500 cities project (Appendix Figure 2) (*15*). We assume that high risk conditions for COVID-19 are the same as those specified for influenza by the CDC (*10*). The CDC's 500 cities project provides city-specific estimates of prevalence for several of these conditions among adults (*16*). The estimates were obtained from the 2015–2016 Behavioral Risk Factor Surveillance System (BRFSS) data using a small-area estimation method known as multilevel regression and poststratification (*11*,*12*). It links geocoded health surveys to high spatial resolution population demographic and socioeconomic data (*12*).

Projected weekly incident COVID-19 cases are shown in Appendix Figure 3, and projected COVID-19 healthcare demand and cumulative deaths are shown in Appendix Figure 4.

Estimating High-Risk Proportions for Adults

To estimate the proportion of adults at high risk for complications, we use the CDC's 500 cities data, as well as data on the prevalence of HIV/AIDS, obesity and pregnancy among adults (Appendix Table 2).

The CDC 500 cities dataset includes the prevalence of each condition on its own, rather than the prevalence of multiple conditions (e.g., dyads or triads). Thus, we use separate co-morbidity estimates to determine overlap. Reference about chronic conditions (*17*) gives US estimates for the proportion of the adult population with 0, 1 or $\geq$2 chronic conditions, per age group. Using this and the 500 cities data we can estimate the proportion of the population p_{HR} in each age group in each city with $\geq$1 chronic condition listed in the CDC 500 cities data (Appendix Table 2) putting them at high risk for flu complications.

HIV

We use the data from Table 20 in a CDC HIV surveillance report (*18*) to estimate the population in each risk group living with HIV in the U.S. (last column, 2015 data). Assuming independence between HIV and other chronic conditions, we increase the proportion of the

population at high-risk for influenza to account for individuals with HIV but no other underlying conditions.

Morbid Obesity

A BMI >40 kg/m^2 indicates morbid obesity and is considered high risk for influenza. The 500 Cities Project reports the prevalence of obese people in each city with BMI > 30 kg/m^2 (not necessarily morbid obesity). We use the data from Table 1 in Sturm and Hattori (*19*) to estimate the proportion of people with a BMI >30 that actually have a BMI >40 (across the United States); we then apply this to the 500 Cities obesity data to estimate the proportion of people who are morbidly obese in each city. Table 1 of Morgan et al. (*20*) suggests that 51.2% of morbidly obese adults have $\geq$1 other high risk chronic condition, and update our high-risk population estimates accordingly to account for overlap.

Pregnancy

We separately estimate the number of pregnant women in each age group and each city, following the methods in the CDC reproductive health report (*21*). We assume independence between any of the high-risk factors and pregnancy, and further assume that half the population are women.

Estimating High-Risk Proportions for Children

Since the 500 Cities Project only reports data for adults $\geq$18 years of age, we take a different approach to estimating the proportion of children at high risk for severe influenza. The 2 most prevalent risk factors for children are asthma and obesity; we also account for childhood diabetes, HIV and cancer.

From Miller et al. (*22*), we obtain national estimates of chronic conditions in children. For asthma, we assume that variation among cities will be similar for children and adults. Thus, we use the relative prevalence of asthma in adults to scale our estimates for children in each city. The prevalence of HIV and cancer in children are taken from CDC HIV surveillance report (*18*) and cancer research report (*23*), respectively.

We first estimate the proportion of children having either asthma, diabetes, cancer or HIV (assuming no overlap in these conditions). We estimate city-level morbid obesity in children using the estimated morbid obesity in adults multiplied by a national constant ratio for each age group estimated from Hales et al. (*24*), this ratio represents the prevalence in morbid obesity in children given the one observed in adults. From Morgan et al. (*20*), we estimate that 25% of morbidly obese children have another high-risk condition and adjust our final estimates accordingly.

Resulting Estimates

We compare our estimates for the Austin-Round Rock Metropolitan Area to published national-level estimates (*25*) of the proportion of each age group with underlying high risk conditions (Appendix Table 9). The biggest difference is observed in older adults, with Austin having a lower proportion at risk for complications for COVID-19 than the national average; for 25–39 year-old the high risk proportion is slightly higher than the national average.

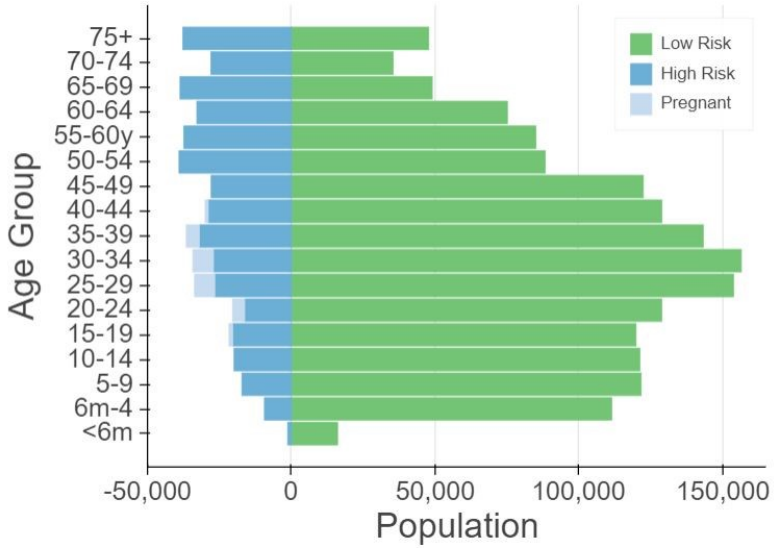

Appendix Figure 2. Demographic and risk composition of the Austin-Round Rock population. Bars indicate age-specific population sizes, separated by low risk, high risk, and pregnant. High risk is defined as individuals with cancer, chronic kidney disease, COPD, heart disease, stroke, asthma, diabetes, HIV/AIDS, and morbid obesity, as estimated from the CDC 500 Cities Project (*15*), reported HIV prevalence (*18*) and reported morbid obesity prevalence (*19*,*20*), corrected for multiple conditions. The population of pregnant women is derived using the CDC's method combining fertility, abortion and fetal loss rates (*26–28*).

Appendix Table 8. High-risk conditions for influenza and data sources for prevalence estimation

Condition	Data source
Cancer (except skin), chronic kidney disease, COPD, coronary heart disease, stroke, asthma, diabetes	CDC 500 cities (*29*)
HIV/AIDS	CDC HIV Surveillance report (*30*)
Obesity	CDC 500 cities (*29*), Sturm and Hattori (*19*), Morgan et al. (*20*)
Pregnancy	National Vital Statistics Reports (*31*) and abortion data (*27*)

Appendix Table 9. Comparison between published national estimates and Austin-Round Rock MSA estimates of the percent of the population at high-risk of influenza/COVID-19 complications

Age group	National estimates (24)	Austin (excluding pregnancy)	Pregnant women (proportion of age group)
<1 to 6 mo	NA	6.8	–
6 mo to 4 y	6.8	7.4	–
5 to 9 y	11.7	11.6	–
10 to 14 y	11.7	13.0	–
15 to 19 y	11.8	13.3	1.7
20 to 24 y	12.4	10.3	5.1
25 to 34 y	15.7	13.5	7.8
35 to 39 y	15.7	17.0	5.1
40 to 44 y	15.7	17.4	1.2
45 to 49 y	15.7	17.7	–
50 to 54 y	30.6	29.6	–
55 to 60 y	30.6	29.5	–
60 to 64 y	30.6	29.3	–
65 to 69 y	47.0	42.2	–
70 to 74 y	47.0	42.2	–
≥75 y	47.0	42.2	–

Section 3. Sensitivity Analysis with Respect to R_0

Our base scenarios assume a basic reproductive number (*R0*) of 2.2. Here, we provide projections assuming that COVID-19 has a higher reproduction number of *R0* = 3.5, with a doubling time of both 4 days and 7.2 days. Assuming this faster transmission scenario, higher levels of social distancing are required to reduce the burden of the disease.

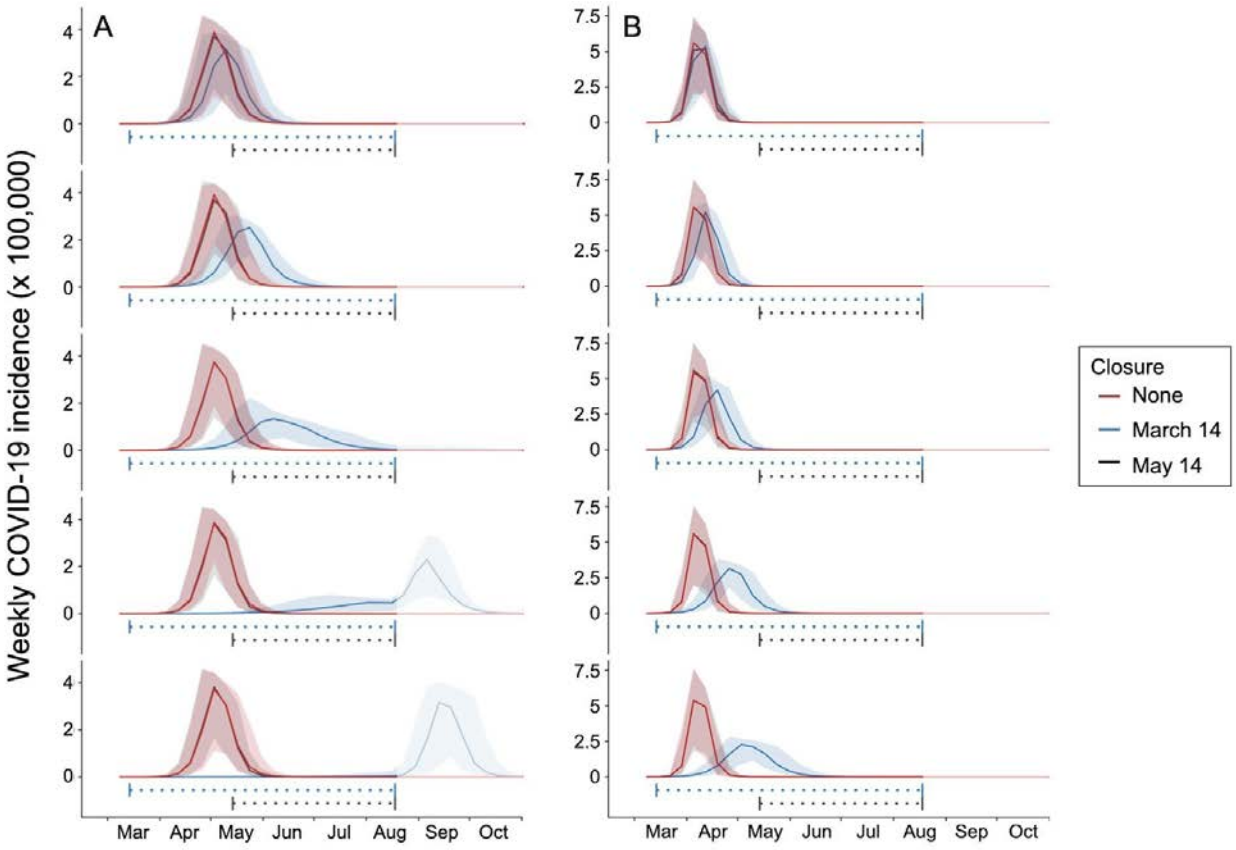

Appendix Figure 3. Projected weekly incident COVID-19 cases in the Austin-Round Rock MSA. Graphs show simulation results for different levels of social distancing and implementation times, assuming R_0 = 3.5 and an epidemic doubling time of A) 7.2 days (*19*–*22*) or B) 4 days (*22*,*24*,*25*). Each graph displays 3 projections: a baseline assuming no social distancing (red), social distancing implemented March 14-Aug 17, 2020 (blue), and social distancing implemented May 14-Aug 17, 2020 (black). From top to bottom, the graphs in each column correspond to increasingly stringent social distancing measures: school closures plus social distancing that reduces nonhousehold contacts by 0%, 25%, 50%, 75%, or 90%. Solid lines indicate the median of 100 stochastic simulations; shading indicates the inner 95% range of values. The horizontal dotted lines beneath the curves indicate intervention periods. The faded mid-August to December time range indicates long-range uncertainty regarding COVID-19 transmission dynamics and intervention policies.

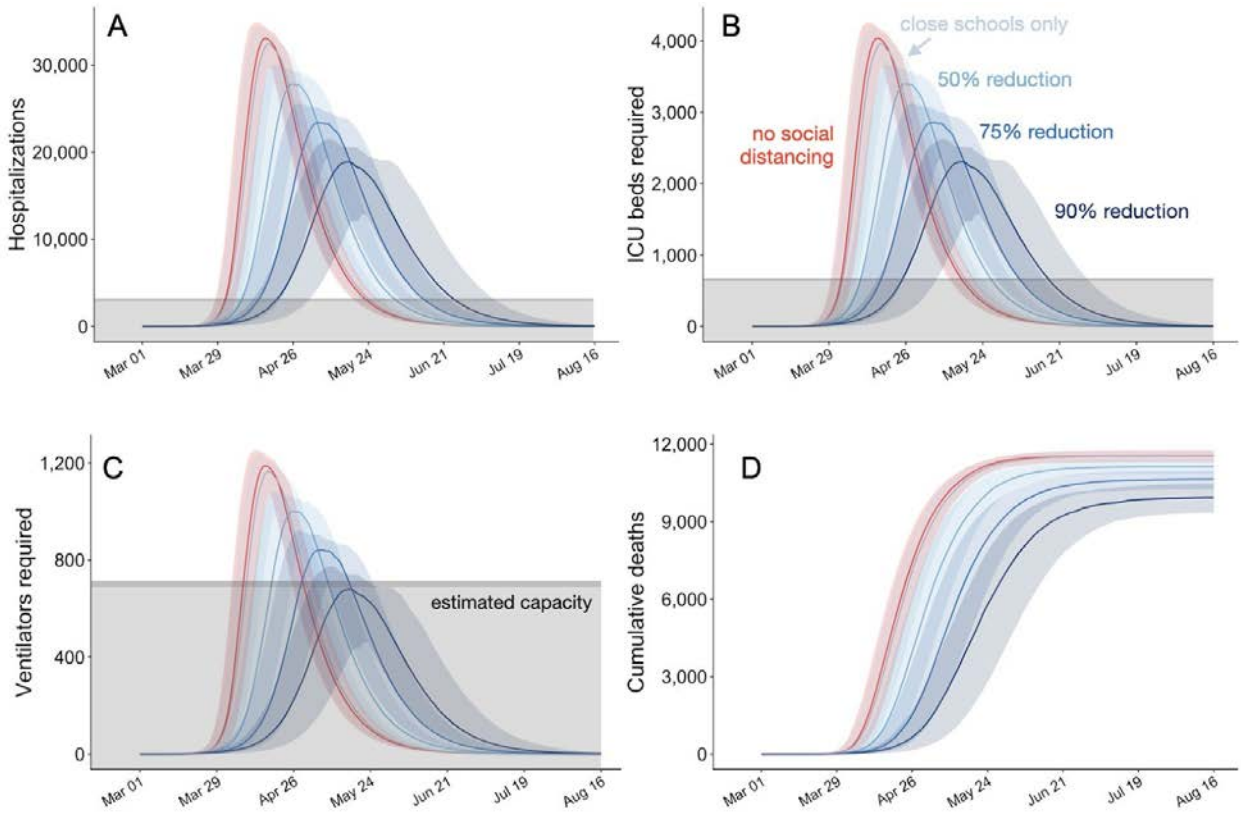

Appendix Figure 4. Projected COVID-19 healthcare demand and cumulative deaths in the Austin-Round Rock MSA from March 1 to August 17, 2020. Graphs show simulation results across multiple levels of social distancing, assuming *R* 0 = 3.5 with a 4-day epidemic doubling time. Extensive social distancing is expected to substantially reduce the burden of COVID-19 A) hospitalizations, B) patients requiring ICU care, C) patients requiring mechanical ventilation, and D) deaths. The red lines project COVID-19 transmission assuming no interventions under the parameters given in Table A1. The blue lines show increasing levels of social distancing interventions, from light to dark: school closures plus social distancing interventions that reduce nonhousehold contacts by either 0%, 50%, 75% or 90%. Lines and shading indicate the median and inner 95% range of values across 100 stochastic simulations. Gray shaded region indicates estimated surge capacity for COVID-19 patients in the Austin-Round Rock MSA as of March 28, 2020, which is calculated based on 80% of 42,99 hospital beds and 90% of 755 ICU beds and 755 mechanical ventilators.

Section 4. Sensitivity Analysis with Respect to Healthcare Durations

With the assumption that the healthcare system is likely to perform less effectively under the highly stressed condition, patient discharge might take longer in the surge setting. As sensitivity analysis, we analyzed longer duration hospital, ICU and ventilator treatment (Appendix Table 10). The results are summarized in Appendix Tables 11, 12 and Appendix Figure 5.

Appendix Table 10. Updated hospitalization parameters for which all values were modified based on discussions with Austin-Round Rock Medical authorities regarding worst case surge scenarios

Parameters	Original	Updated for sensitivity analysis	Details
γ^H: recovery rate in hospitalized compartment	0.0869565	0.07142857	14 d average from admission to discharge
μ: rate from hospitalized to death	0.0892857	0.07142857	14 d average from admission to death
Vent: proportion of individuals in ICU needing ventilation	0.35, 0.3, 0.45, 0.5, 0.45	0.67 (all ages)	
d_{ICU} : duration of stay in ICU	8 d	14 d	
d_V : duration of ventilation	5 d	10 d	

Appendix Table 11. Longer treatment surge scenario: estimated cumulative COVID-19 cases, healthcare requirements and deaths. The values are medians (with 95% prediction interval in parentheses) across 100 stochastic simulations for the Austin-Round Rock MSA from March 1 through August 17, 2020 based on the parameters given in Appendix Table 10

Outcome	No measures	School closure	School closure and 50% social distancing	School closure and 75% social distancing	School closure and 90% social distancing
Hospitalizations	79,788 (75,891-82,399)	76,873 (71,552-80,870)	40,719 (17,031-57,014)	2,120 (148-9,939)	118 (14-546)
ICU	13,415 (12,775-13,859)	12,919 (12,025-3,587)	6,841 (2,859-9,581)	356 (25-1,673)	20 (2-92)
Ventilators	8,943(8,517-9,239)	8,612 (8,016-9,058)	4,561 (1,906-6,388)	237 (17-1,115)	13 (2-61)

Appendix Table 12. Longer treatment surge scenario: estimated peak COVID-19 healthcare demands. The values are medians (with 95% prediction interval in parentheses) across 100 stochastic simulations for the Austin-Round Rock MSA from March 1 through August 17, 2020 based on the parameters given in Appendix Table 10

Outcome	No measures	School closure	School closure and 50% social distancing	School closure and 75% social distancing	School closure and 90% social distancing
Hospitalizations	27,678 (25,651-29,286)	25,347 (21,806-27,588)	8,862 (5,164-12,492)	564 (30-2,953)	22 (4-117)
ICU	4,669 (4,323-4,944)	4,273 (3,673-4,649)	1,488 (868-2,101)	95 (5-496)	4 (1-20)
Ventilators	2,223 (2,059-2,354)	2,035 (1,749-2,214)	709 (413-1,000)	45 (2-236)	2 (0-9)

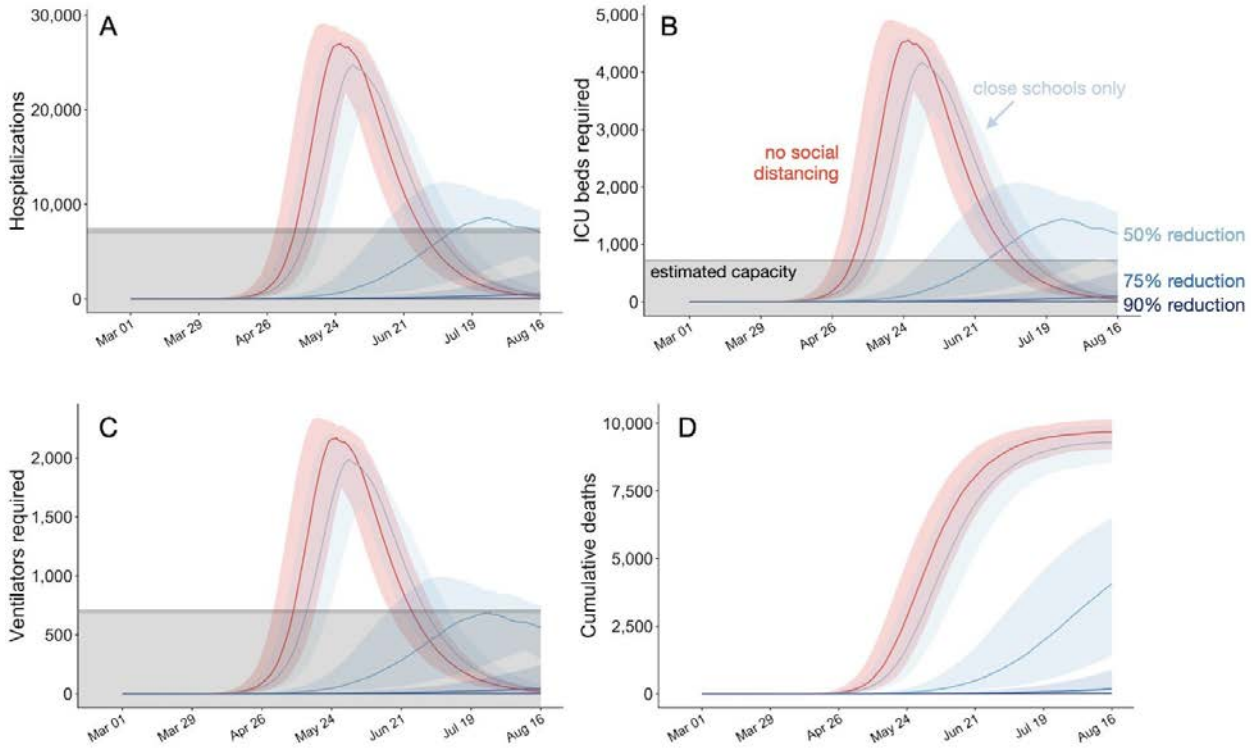

Appendix Figure 5. Longer treatment surge scenario: projected COVID-19 healthcare demand and cumulative deaths in the Austin-Round Rock MSA from March 1 to August 17, 2020. Graphs show simulation results across multiple levels of social distancing, assuming *R* 0 = 2.2 with a 4-day epidemic doubling time. Extensive social distancing is expected to substantially reduce the burden of COVID-19 A) hospitalizations, B) patients requiring ICU care, C) patients requiring mechanical ventilation, and D) deaths. The red lines project COVID-19 transmission assuming no interventions under the parameters given in Table A1. The blue lines show increasing levels of social distancing interventions, from light to dark: school closures plus social distancing interventions that reduce nonhousehold contacts by either 0%, 50%, 75% or 90%. Lines and shading indicate the median and inner 95% range of values across 100 stochastic simulations. Gray shaded region indicates estimated surge capacity for COVID-19 patients in the Austin-Round Rock MSA as of March 28, 2020, which is calculated based on 80% of 4,299 hospital beds and 90% of 755 ICU beds and 755 mechanical ventilators.

Section 5. Impact of 2-Week and 4-Week Delays in Implementation of Social Distancing Interventions, 2020.

We also modeled intermediate delays of 2 weeks (March 28) and 4 weeks (April 11). Even 2-week delays undermine the efficacy of the interventions with respect to reducing healthcare demand below local capacity (Appendix Figure 6, Appendix Table 13).

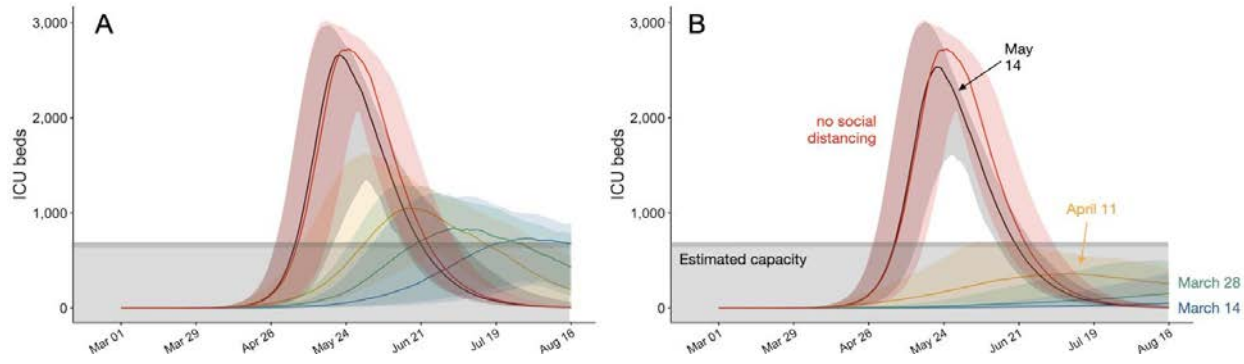

Appendix Figure 6. Graphs show simulation results for school closures with A) 50% reduction in nonhousehold contacts and B) 75% reduction in nonhousehold contacts, assuming *R* 0 = 2.2 with a 4-day epidemic doubling time. The red lines project COVID-19 transmission assuming no interventions under the parameters given in Appendix Table 1. The other lines colors indicate different delays in the timing of intervention: blue, green, yellow and black correspond to March 14, March 28, April 11, and May 14, 2020, respectively. Lines and shading indicate the median and inner 95% range of values across 100 stochastic simulations. Gray shaded region indicates estimated surge capacity for COVID-19 patients in the Austin-Round Rock MSA as of March 28, 2020, which is calculated based on 90% of 755 ICU beds.

Appendix Table 13. Date when COVID-19 healthcare requirements exceed capacity based on implementation date for school closures with 50% or 75% social distancing. Each value is a median across 100 stochastic simulations for the Austin-Round Rock MSA before August 17, 2020, based on the parameters given in Appendix Table 1

	School closure and 50% social distancing			School closure and 75% social distancing		
Outcome	March 14 start	March 28 start	April 11 start	March 14 start	March 28 start	April 11 start
Hospitalizations	July 1	June 7	May 23	Not exceed	Not exceed	Not exceed
ICU	July 20	June 20	May 31	Not exceed	Not exceed	Not exceed

References

1. Keeling MJ, Rohani P. Modeling infectious diseases in humans and animals. Princeton (NJ): Princeton University Press; 2011.

2. Gillespie DT. Approximate accelerated stochastic simulation of chemically reacting systems. J Chem Phys. 2001;115:1716–33. https://doi.org/10.1063/1.1378322

3. Li Q, Guan X, Wu P, Wang X, Zhou L, Tong Y, et al. Early transmission dynamics in Wuhan, China, of novel coronavirus-infected pneumonia. N Engl J Med. 2020;382:1199–207. PubMed https://doi.org/10.1056/NEJMoa2001316

4. Kraemer MU, Yang C-H, Gutierrez B, Wu C-H, Klein B, Pigott DM, et al.; Open COVID-19 Data Working Group. The effect of human mobility and control measures on the COVID-19 epidemic in China. Science. 2020;368:493–7. PubMed https://doi.org/10.1126/science.abb4218

5. He X, Lau EH, Wu P, Deng X, Wang J, Hao X, et al. Temporal dynamics in viral shedding and transmissibility of COVID-19. Nat Med. 2020;26:672–5. PubMed https://doi.org/10.1038/s41591-020-0869-5

6. Gudbjartsson DF, Helgason A, Jonsson H, Magnusson OT, Melsted P, Norddahl GL, et al. Spread of SARS-CoV-2 in the Icelandic population. N Engl J Med. 2020;382:2302–15. PubMed https://doi.org/10.1056/NEJMoa2006100

7. Zhang J, Litvinova M, Wang W, Wang Y, Deng X, Chen X, et al. Evolving epidemiology and transmission dynamics of coronavirus disease 2019 outside Hubei province, China: a descriptive and modelling study. Lancet Infect Dis. 2020;20:793–802. PubMed https://doi.org/10.1016/S1473-3099(20)30230-9

8. He D, Zhao S, Lin Q, Zhuang Z, Cao P, Wang MH, et al. The relative transmissibility of asymptomatic COVID-19 infections among close contacts. Int J Infect Dis. 2020;94:145–7. PubMed https://doi.org/10.1016/j.ijid.2020.04.034

9. Verity R, Okell LC, Dorigatti I, Winskill P, Whittaker C, Imai N, et al. Estimates of the severity of coronavirus disease 2019: a model-based analysis. Lancet Infect Dis. 2020;20:669–77. PubMed https://doi.org/10.1016/S1473-3099(20)30243-7

10. Centers for Disease Control and Prevention. People at high risk of flu, 2019 [cited 2020 Mar 26]. https://www.cdc.gov/flu/highrisk/index.htm

11. Centers for Disease Control and Prevention. Behavioral risk factor surveillance system, 2019 [cited 2020 Mar 26]. https://www.cdc.gov/brfss/index.html

12. Zhang X, Holt JB, Lu H, Wheaton AG, Ford ES, Greenlund KJ, et al. Multilevel regression and poststratification for small-area estimation of population health outcomes: a case study of chronic obstructive pulmonary disease prevalence using the behavioral risk factor surveillance system. Am J Epidemiol. 2014;179:1025–33. PubMed https://doi.org/10.1093/aje/kwu018

13. Austin ISD. Calendar of events [cited 2020 Mar 26]. https://www.austinisd.org/calendar

14. SciPy Community. minimize(method='trust-constr') — SciPy v1.4.1 Reference Guide [cited 2020 Mar 28]. https://docs.scipy.org/doc/scipy/reference/optimize.minimize-trustconstr.html

15. Centers for Disease Control and Prevention. 500 cities project: local data for better health, 2019 [cited 2020 Mar 19]. https://www.cdc.gov/500cities/index.htm

16. Centers for Disease Control and Prevention. Health outcomes: 500 cities, 2019 [cited 2020 Mar 28]. https://www.cdc.gov/500cities/definitions/health-outcomes.htm

17. PEW Research. Part one: who lives with chronic conditions, 2013 [cited 2019 Nov 23]. https://www.pewresearch.org/internet/2013/11/26/part-one-who-lives-with-chronic-conditions/

18. Centers for Disease Control and Prevention. HIV surveillance report, 2016; 2018 [cited 2020 Jul 15] https://www cdc gov/hiv/library/reports/hiv-surveil-lance html

19. Sturm R, Hattori A. Morbid obesity rates continue to rise rapidly in the United States. Int J Obes. 2013;37:889–91. PubMed https://doi.org/10.1038/ijo.2012.159

20. Morgan OW, Bramley A, Fowlkes A, Freedman DS, Taylor TH, Gargiullo P, et al. Morbid obesity as a risk factor for hospitalization and death due to 2009 pandemic influenza A(H1N1) disease. PLoS One. 2010;5:e9694. PubMed https://doi.org/10.1371/journal.pone.0009694

21. Centers for Disease Control and Prevention, Division of Reproductive Health. Estimating the number of pregnant women in a geographic area [cited 202 Jul 15]. https://www.cdc.gov/reproductivehealth/emergency/pdfs/PregnacyEstimatoBrochure508.pdf

22. Miller GF, Coffield E, Leroy Z, Wallin R. Prevalence and costs of five chronic conditions in children. J Sch Nurs. 2016;32:357–64. PubMed https://doi.org/10.1177/1059840516641190

23. American Cancer Society. Cancer facts and figures, 2014 [cited 2020 Mar 30]. https://www.cancer.org/research/cancer-facts-statistics/all-cancer-facts-figures/cancer-facts-figures-2 014.html

24. Hales CM, Fryar CD, Carroll MD, Freedman DS, Ogden CL. Trends in obesity and severe obesity prevalence in US youth and adults by sex and age, 2007–2008 to 2015. JAMA. 2018;319:1723–5. PubMed https://doi.org/10.1001/jama.2018.3060

25. Zimmerman RK, Lauderdale DS, Tan SM, Wagener DK. Prevalence of high-risk indications for influenza vaccine varies by age, race, and income. Vaccine. 2010;28:6470–7. PubMed https://doi.org/10.1016/j.vaccine.2010.07.037

26. Martin JA, Hamilton BE, Osterman MJK, Driscoll AK, Drake P. Births: final data for 2017. Natl Vital Stat Rep. 2018;67:1–50. PubMed

27. Jatlaoui TC, Boutot ME, Mandel MG, Whiteman MK, Ti A, Petersen E, et al. Abortion surveillance—United States, 2015. MMWR Surveill Summ. 2018;67:1–45. PubMed https://doi.org/10.15585/mmwr.ss6713a1

28. Ventura SJ, Curtin SC, Abma JC, Henshaw SK. Estimated pregnancy rates and rates of pregnancy outcomes for the United States, 1990-2008. Natl Vital Stat Rep. 2012;60:1–21. PubMed

29. Centers for Disease Control and Prevention. 500 cities project: local data for better health, 2019 [cited 2020 Jun 22]. https://www.cdc.gov/500cities/index.htm

30. Centers for Disease Control and Prevention. Health outcomes: 500 cities, 2019 [cited 2020 Jun 22]. https://www.cdc.gov/500cities/definitions/health-outcomes.htm

31. Martin JA, Hamilton BE, Osterman MJ, Driscoll AK, Drake P. Births: Final Data for 2017. Natl Vital Stat Rep. 2018;67:1–50. PubMed